ELSEVIER

Contents lists available at ScienceDirect

Materials Today Communications

journal homepage: www.elsevier.com/locate/mtcomm



Materials characterization of Ti6Al4V to NbZr1 bimetallic structure fabricated by wire arc additive manufacturing

Sainand Jadhav ^a, Mahdi Sadeqi Bajestani ^a, Saiful Islam ^a, Md Abdul Karim ^a, Chang Jong Kim ^b, Ho-Jin Lee ^c, Young Tae Cho ^b, Duck Bong Kim ^{d,*}

- ^a Department of Mechanical Engineering, Tennessee Technological University, Cookeville, TN, USA
- ^b Department of Smart Manufacturing Engineering, Changwon National University, Changwon, South Korea
- ^c Smart Manufacturing Technology R&D Group, Korea Institute of Industrial Technology, Daegu, South Korea
- ^d Department of Manufacturing and Engineering Technology, Tennessee Technological University, Cookeville, TN, USA

ARTICLEINFO

Keywords: Bimetallic structures Wire arc additive manufacturing Refractory alloys NbZr1 Ti6Al4V

ABSTRACT

This study investigated the microstructures and mechanical properties of a bimetallic structure (BS) of a titanium alloy (Ti6Al4V) and a niobium alloy (NbZr1) manufactured by wire arc additive manufacturing (WAAM). Three BS thin-walls were deposited with different heat input conditions: low (180 amperes (A)), medium (200 A), and high (220 A). Microstructural characterization at the interface showed that the Niobium (Nb) diffusion on the Ti6Al4V side increased as the heat input was increased. The interfacial microstructure comprised an island area and a dendritic zone with solid solutions of (β Ti and Nb) and ($\alpha + \beta$ Ti and Nb), respectively. The hardness ranged from 99 to 367 Vickers Hardness (HV), with a considerable decrease at the interface due to the migration of Nb. Maximum ultimate tensile strength of 567 MPa was achieved for the low heat input sample, and the failure occurred at the NbZr1 side. The fractography revealed intergranular and transgranular fracture morphologies, indicating a brittle failure. The results showed that the proposed BS has a good bonding strength, and neither defects (e.g., pores and cracks) nor intermetallic compounds were observed at the interface.

1. Introduction

Additive manufacturing (AM) employs layer-by-layer deposition and is particularly suited for fabricating dissimilar metals into a single component, called "bimetallic structure (BS)" [1]. Niobium-zirconium (NbZr1), one of the refractory alloys, is widely used in extreme environments (e.g., nuclear reactors) due to its extraordinary physicochemical properties, including high-temperature strength and high ductility [2,3]. In addition, Ti6Al4V, one of the titanium (Ti) alloys, is a high-performance alloy with a high strength-to-weight ratio. It is used for a wide range of applications where low density and excellent corrosion resistance are necessary (e.g., aerospace industry) [4]. Provided these two alloys are joined into a single part, their unique characteristics can complement each other, enhancing their multifunctional capabilities and enabling a broad range of potential applications [1].

The Ti6Al4V-NbZr1 BS can be manufactured through traditional processes, e.g., welding, brazing, and diffusion bonding. These processes have critical issues, including heat-affected zone, heterogeneity at the interface, and cracking due to brittle phase formation [1]. Torkamany

et al. [5] investigated the effects of laser pulse energy, duration, and repetition rates on the melt pool in pulsed laser-welded Ti6Al4V-Nb sheets. The bonding strength of 269 MPa was achieved with the absence of intermetallic compounds (IMCs). Siqueira et al. [6] studied the microstructure and hardness of fiber laser beam welded Ti-Nb sheets. The samples were defect-free, and the hardness profile decreased from the top (Ti) to the bottom (Nb). Franchini et al. [7] also successfully welded a Nb-base alloy (C-103) to Ti6Al4V without cracks using electron beam welding, achieving tensile strength of 511 MPa. Gao et al. [8, 9] observed that no IMC was formed during the laser welding of pure Ti to Nb sheets. Shehbaz et al. [10] investigated the influence of Nb as an interlayer on the microstructure evolution, mechanical characteristics, and interfacial strength of dissimilar CpTi and IN718 TIG weldment. Nb interlayer suppressed the interdiffusion of Ti and Ni across the interlayer resulting in no TixNiy intermetallic compounds (IMCs) at the CpTi/IN718 dissimilar joint.

Various BSs, for example, steel-bronze, steel-aluminum alloys, steel-nickel/nickel alloys, steel-copper, and copper-titanium, have been successfully fabricated via metal AM [1,11]. Metal AM can be

E-mail address: dkim@tntech.edu (D.B. Kim).

^{*} Corresponding author.

Table 1Elemental composition (wt%) of NbZr1 wire used in this study.

Element	Nb	Zr	Ta	О	W	Mo	Hf	C	N	Fe	Al	Si	Ni
Composition (w%)	Bal.	0.8-1.2	0.5	0.025	0.05	0.05	0.02	0.01	0.01	0.01	0.005	0.005	0.005

Table 2Constant process parameters.

Process parameters	Value			
Wire diameter	0.95 mm			
Substrate dimension	$120\times10\times32~\text{mm}^3$			
Travel speed (TS)	200 mm/min			
Wire feed rate (WFR)	1500 mm/min			
Electrode-to-workpiece distance	5 mm			
Electrode tip angle	45°			
Torch angle	90°			
Shielding gas flow rate	15 L/min			

Table 3Process parameters for different heat input conditions.

Condition	Current (A)	Heat input (J/mm)	Energy density (J/mm³)
LHI	180	810	138
MHI	200	900	153
HHI	220	990	168

categorized into powder-bed, powder-fed, and wire-fed processes [12]. Wire arc additive manufacturing (WAAM), one of the wire-fed processes, uses an electric arc as an energy source to melt the wire feedstock [13]. It can be further classified as gas tungsten arc welding (GTAW), gas metal arc welding (GMAW), and plasma arc welding (PAW). It can provide the fabrication capability of multi-materials and functionally-graded materials (FGMs) [11,14]. Its unique features (e.g., high deposition rate, low capital cost, and high energy density/efficiency [14]) have provided great potential for fabricating BS of refractory alloys (e.g., NbZr1) and high-performance alloys (e.g., Ti6Al4V).

In this paper, we aim to investigate the microstructural characteristics and mechanical properties of bimetallic thin-wall structures of Ti6Al4V-NbZr1 fabricated by wire arc additive manufacturing with respect to different heat input conditions. Using electron microscopy and elemental mapping, microstructures of the bimetallic structures were characterized with a focus on the interface. In addition, microhardness, tensile tests, and fractured surfaces were investigated to extract the mechanical properties.

2. Materials and method

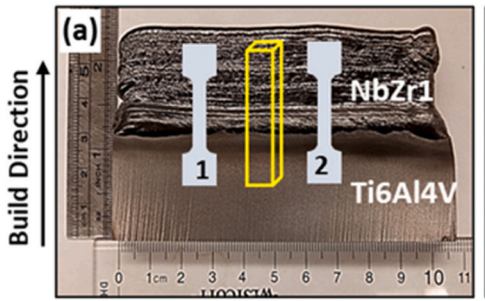
A GTAW-based WAAM system was utilized, which consists of a 6-axis Fanuc ArcMate 120iC robot with a Fanuc R-J3iB controller, a Miller Dynasty 400 GTA welding power source, and a generic wire feeder [15]. NbZr1 alloy wire (ASTM-B392) with a diameter of 0.95 mm was used for the deposition. The elemental composition of the wire is provided in Table 1 [16]. The NbZr1 was deposited on the Ti6Al4V substrate of 120 \times 10 \times 32 mm³. Travel speed (200 mm/min), wire feed rate (1500 mm/min), electrode-to-workpiece distance (5 mm), electrode tip angle (45°), torch angle (90°), and the shielding gas flow rate (15 L/min) were kept constant in all experiments, as listed in Table 2. In addition to shielding gas with the composition of 70 % argon and 30 % helium, trailing gas of 99.99 % argon was used to prevent oxidation after the deposition of each layer. The welding voltage depends on the electrode-to-workpiece distance, so all experiments were carried out with a constant gap of 5 mm to maintain consistency.

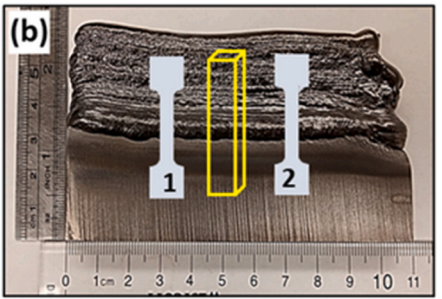
The deposition conditions of the thin-walls are based on the heat input and are controlled by the arc current: low heat input (LHI) for 180 A, medium heat input (MHI) for 200 A, and high heat input (HHI) for 220 A. The details of the process parameters are listed in Table 3. Energy density and heat input are calculated using Eqs. (1 and 2) [17]. The interpass temperature was maintained at 100 $^{\circ}$ C throughout the experiment. Fig. 1 shows the three thin-walls. The height and number of layers are; 58 mm and 25 for LHI, 57 mm and 29 for MHI, and 55 mm and 34 for HHI conditions, respectively.

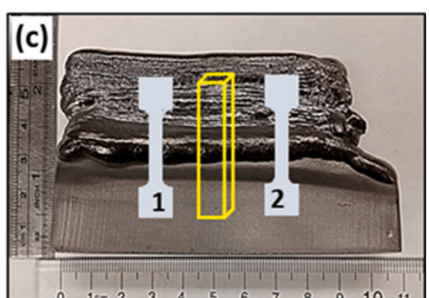
$$Heat input(J/mm) = \frac{Current \times Voltage \times 60}{TS}$$
 (1)

Energy density(J/mm³) =
$$\frac{Current \times Voltage \times 60}{\pi \times (wire \ radius)^2 \times WFS}$$
 (2)

After deposition, the bimetallic structures were sectioned along the build direction, as shown by the yellow region in Fig. 1(a), to prepare samples for microstructures and microhardness tests. The samples were hot-mounted, grounded, and polished following standard metallographic procedure. The Ti6Al4V sides of polished samples were etched with 3 mL HF + 5 mL HNO $_3$ + 100 mL H $_2$ O, and the NbZr1 sides were etched with 10 mL HF + 20 mL HNO $_3$ + 10 mL H $_2$ O. The microstructures and fractured surfaces were analyzed using Nikon Epiphot inverted optical microscope (OM), FEI Quanta 200, and Hitachi SU 7000 scanning electron microscope (SEM) coupled with energy dispersive spectrometry (EDS). For EDS analysis EDAX Octane Elect Super EDS system







Deposition Direction

Fig. 1. Multi-layer thin-walls of Ti6Al4V-NbZr1 fabricated in (a) LHI, (b) MHI, and (c) HHI conditions.

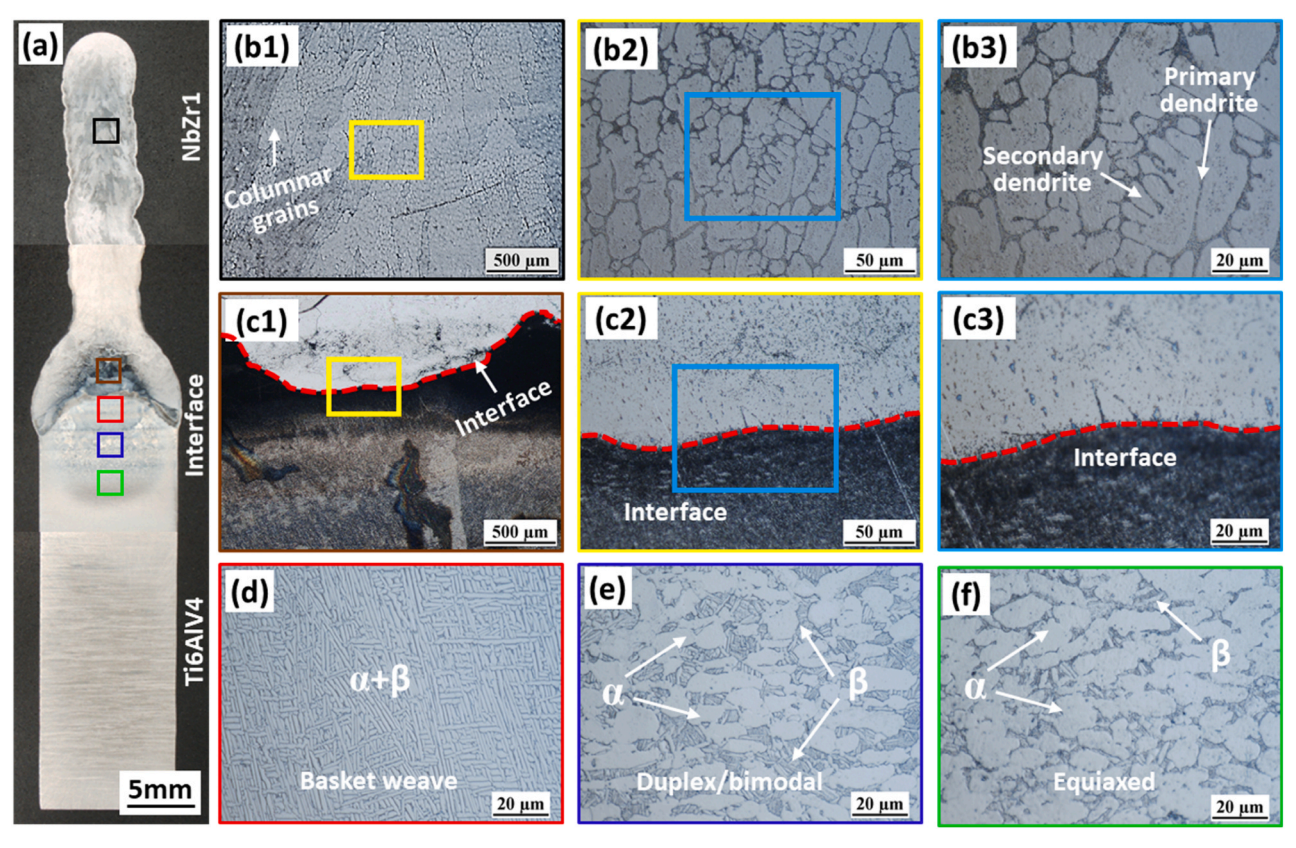


Fig. 2. Optical microscopy images showing the microstructure of Ti6Al4V-NbZr1 BS fabricated in LHI condition: (a) overall cross section, (b1) - (b3) the NbZr1 side, (c1) - (c3) the interface, and (d) - (f) the Ti6Al4V side.

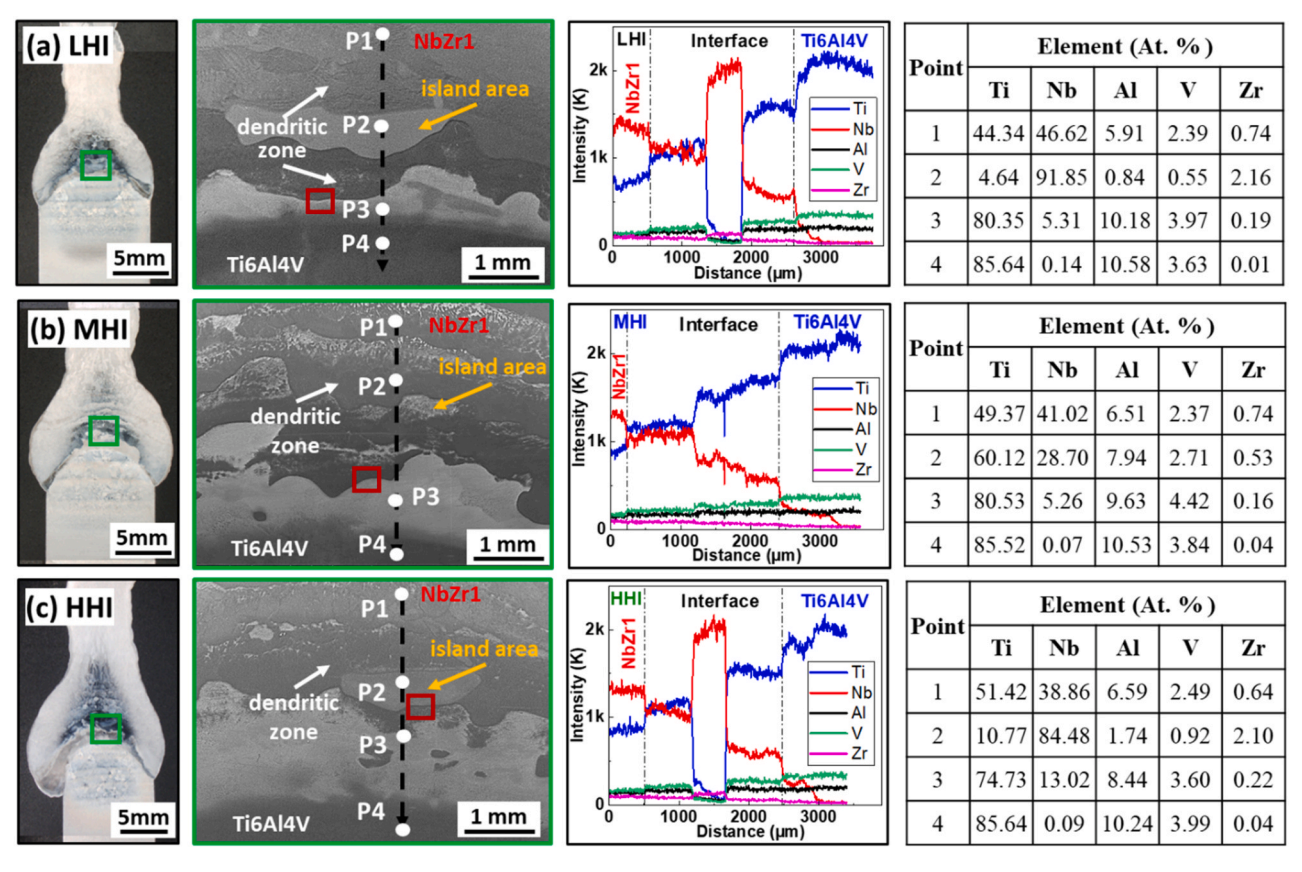


Fig. 3. EDS line and point scan results at the interface for the (a) LHI, (b) MHI, and (c) HHI conditions.

with EDAX APEX software was used. X-ray diffraction (XRD) analysis was also carried out utilizing the Rigaku Ultima IV machine to determine the phases at the interface. In addition, microhardness tests were performed along the build direction of thin-walls using a Buehler-Wilson VH1202 with a 500 g load and a dwell time of 10 s. Two tensile specimens were prepared from each thin-wall using wire electrical discharge machining having a gauge section dimension of (10.16 \times 3.175 \times 2 mm³). Tensile tests were conducted on the TestResources 810 E4 Electrodynamic test machine using a strain rate of 0.001 s $^{-1}$.

3. Results and discussion

3.1. Microstructure analysis

The microstructural features of the NbZr1 side, the interface region, and the Ti6Al4V side for three deposited thin-walls were investigated. Since similar characteristics were found in each condition, only the micrographs of the LHI condition are explained. Fig. 2(a) shows the overall cross-sectional image of the BS. The top portion of the deposit is the NbZr1 which consists of a columnar grain, with grains elongated towards the build direction, as shown in Fig. 2(b1). Magnified images in Fig. 2(b2) and (b3) also reveal the formation of primary and secondary dendrites in that region. Similar results were also found in the literature [17] The Ti6Al4V-NbZr1 interface is presented in Fig. 2(c1). The interface is marked with a red line for better visualization. Higher magnification images in Fig. 2(c2) and (c3) confirm that no cracks, pores, or IMCs were formed at the interface. Fig. 2(d) - (f) show the microstructure of the Ti6Al4V side. The microstructure varies from basket weave-like to duplex/bimodal and equiaxed based on the location. Differences in the microstructure can be attributed to variations in the heat affected zone. Typically, Ti6Al4V microstructure contains fine acicular α and β and prior β grain boundaries. The microstructure of the Ti6Al4V substrate just below the interface shows a coarse β columnar, with α lamellae arranged in a basket weave structure as depicted in Fig. 2(d). A similar microstructure was observed by Patrizia et al. [18].

Fig. 3 shows the SEM images of the interface for three different heat input conditions. The microstructure at the interface comprises an island area and a dendritic zone with solid solutions of (β Ti and Nb) and ($\alpha + \beta$ Ti and Nb), respectively. Gao et al. [8] observed similar microstructures for pulsed laser-welded Ti6Al4V-Nb dissimilar alloys. The formation of island areas is due to the difference in melting point of Ti6al4V and NbZr1 and the fluid flow of the molten pool. According to the Ti-Nb binary phase diagram [19], the melting point of the mixed Ti-Nb molten metal increases as the Nb content rises. Accordingly, within the melt pool, the zones with higher Nb content have higher melting points and are solidified earlier; thus, they form island areas. However, zones with higher Ti content solidify later, forming dendritic zone. To verify this, an EDS line and point scan analysis were carried out at four different locations, as shown in Fig. 3. The heterogeneous Ti, Al, V, and Nb distribution along the scan line indicates the lack of Ti and Nb mixing in the melt pool. This could result from the difference in composition of dissimilar metals and an intense fluid flow in the melt pool due to the temperature gradient and surface tension [20,21]. Point analysis for P4, which is on the Ti6Al4V side, shows a major concentration of Ti with a very small quantity of Nb and Zr in each condition heat input condition. The Nb content at P2, located on the island, is greater than 75 %, but it is less than 30 % at P2, located in the dendritic zone. This indicates macro-segregation at the interface. However, at P1, which is close to the NbZr1 side, Ti concentration is more than 40 %, indicating Ti is diffused into the NBZr1 side.

Fig. 4(a) - (c) show the magnified SEM images of the region marked with red rectangle in Fig. 3 and the corresponding EDS area map. From

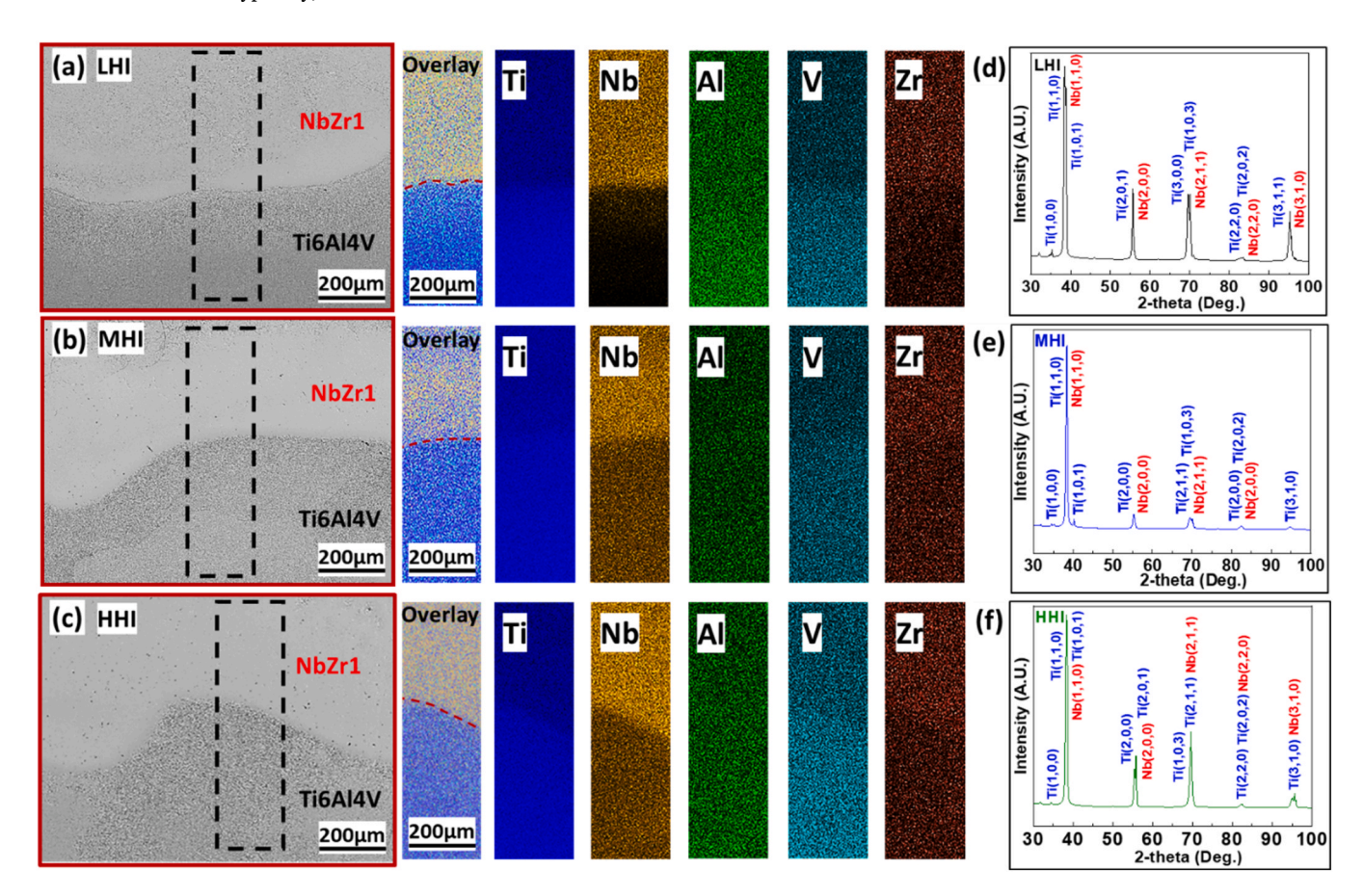


Fig. 4. SEM images of the interface along with elemental area mapping for the (a) LHI, (b) MHI, and (c) HHI condition; the XRD results at the interface for the (d) LHI, (e) MHI, and (f) HHI condition.

the overlay images, it is observed that Ti, Al, and V are concentrated at the bottom, while Nb and Zr are concentrated at the top. In addition, the diffusion of Ti into the NbZr1 region is shown as blue spots. Migration of Nb to the Ti6Al4V is also observed. The results showed that as the heat input rises and the temperature of the melt pool increases, more Nb is diffused into the Ti6Al4V side. Fig. 4(d) - (f) show the XRD pattern of the interface region carried out for a scan range of $2\theta = 30-100^\circ$. Major peaks and corresponding crystal planes are identified. They show the existence of Ti and Nb phases without IMC formation. Based on the binary phase diagrams of Ti-Nb and Nb-V [19] and the ternary phase diagram of Ti-Nb-Al (below 7.5 wt% Al), no IMC is observed [22]. Accordingly, no IMC is formed at the interface, and XRD results confirm this. Major peaks are observed at $2\theta \sim 35^\circ$, 38° , 55° , 69° , 83° , and 95° in all conditions indicating that the heat input does not significantly affect the location of the peaks.

3.2. Mechanical test

The microhardness tests were performed along the build direction at a spacing of 1.0 mm for Ti6Al4V and NbZr1 and 0.25 mm for the interface, and the results are presented in Fig. 5. For all heat input conditions, the average hardness has the highest value at the Ti6Al4V substrate and the lowest at the interface. The maximum hardness value on the Ti6Al4V side reaches 367.3 HV, close to that of the Ti6Al4V base metal. The hardness value ranges from 99.9 HV to 339 HV at the interface region. The hardness at the interface randomly fluctuates due to the microstructural heterogeneities and variations of local composition at each hardness measurement point. The zones containing higher amounts of Ti are expected to have higher hardness. Minimum hardness values observed at the interface are 99 HV, 202 HV, and 121 HV for LHI, MHI, and HHI, respectively. Reduction in hardness at the interface revealed that no hard or brittle IMC is formed during deposition. On the NbZr1 side, hardness varied from 162 HV to 321 HV, which is comparatively higher than the conventionally fabricated NbZr1 (121.5 \pm 2.4 HV) [23]. In addition, on the NbZr1 side, the hardness increased in the build direction. In WAAM NbZr1, a similar trend has been found in the literature [17]. The paper correlated the increases in hardness value with the decrease of the secondary dendritic arm spacing (SDAS). This is because the top layers go through a smaller number of thermal cycles and heat transfer is comparatively faster. This phenomenon promotes smaller SDAS and increases the hardness.

The stress-strain curves for three heat input conditions, along the fractured tensile samples, are illustrated in Fig. 6(a) - (c). The average tensile strength of 543.5 MPa, 393 MPa, and 367.5 MPa were measured for LHI, MHI, and HHI, respectively. It is observed that the tensile strength increases as the heat input decreases. All samples failed on the NbZr1 side, indicating relatively good bonding at the Ti6Al4V/NbZr1 interface. The fracture location is in accordance with the findings of Torkamany et al. [5] and Franchini et al. [7] for electron beam welding of Ti6Al4V to C103 and laser welding of pure Nb to Ti6Al4V, respectively. As sample failed on the NbZr1 side, to some extent, the strength of the Ti6Al4V-NbZr1 bimetallic structure could be compared to the strength of conventional and additively manufactured NbZr1 alloy. A previous study [17] on WAAM-based NbZr1 demonstrated maximum tensile strength of 412 MPa, while the Ti6Al4V-NbZr1 bimetallic structure achieved average tensile strength of 543.5 MPa for LHI condition in the current study. The strength is also comparable to other manufacturing methods of NbZr1 [17]. However, the strain was very low (less than 4 %) as compared to the previous studies on NbZr1 alloy [17], resulting the samples experienced a brittle fracture. Fig. 6(d) - (i) represent the lower magnification fractography images. The LHI condition samples exhibited intergranular and transgranular fracture morphologies, as shown in Fig. 6(d) and (g). However, in MHI samples, an entirely intergranular fracture surface was observed, as evidenced by the rock candy pattern in Fig. 6(e) and (h). For the HHI condition, a transgranular fracture by quasi-cleavage and a relatively flat surface with

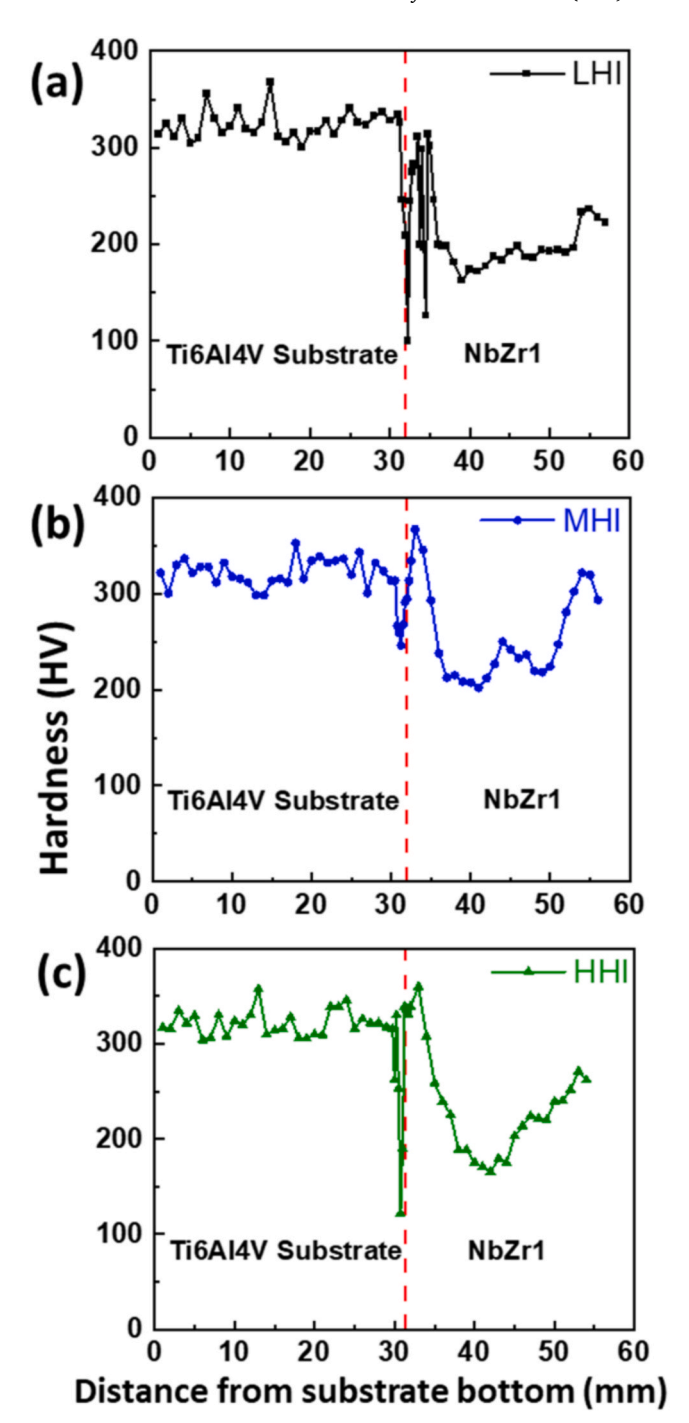


Fig. 5. Hardness profiles of the Ti6Al4V-NbZr1 BS for the (a) LHI, (b) MHI, and (c) HHI condition.

river patterns were observed, as illustrated in Figs. (f) and (i). No significant correlation between heat input condition and fracture morphology was observed. Further investigations are required to evaluate the influence of heat input on fracture behavior.

4. Conclusion

This study demonstrated the feasibility of fabricating Ti6Al4V-NbZr1 BS by WAAM and investigated the microstructures and mechanical properties in three heat input conditions. The following conclusions can be drawn from the study:

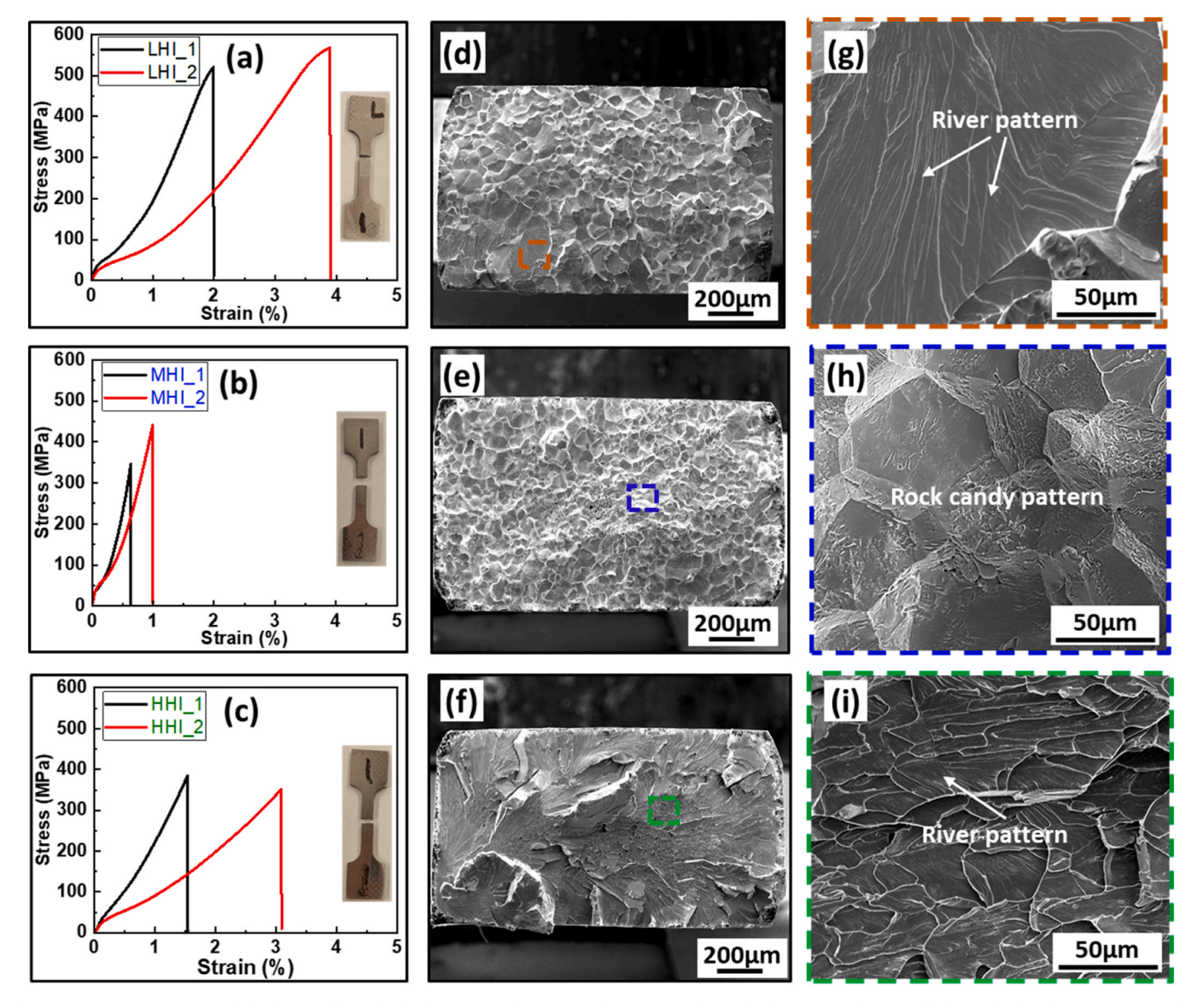


Fig. 6. Stress-strain curves with the fractured sample for the (a) LHI, (b) MHI, and (c) HHI condition; the fracture surface morphologies for the (d) - (g) LHI, (e) - (h) MHI, and (f) - (i) HHI condition.

- Neither defects (i.e., pores and cracks) nor IMC formation are observed at the interface of the BS in three heat input conditions.
- The interfacial microstructures comprise an island area and a dendritic zone with solid solutions of (β Ti, Nb) and ($\alpha + \beta$ Ti, Nb), respectively.
- The lower hardness at the interface is due to the presence of Nb. Fluctuations in the hardness along the interface are due to variations in local composition. The increasing trend in the hardness value was observed on the NbZr1 side.
- The maximum ultimate tensile strength of 567 MPa is achieved in the LHI condition, comparable to the conventionally and additively manufactured NbZr1. With a decrease in the heat input, an increase in the ultimate tensile strength is observed.
- The failure occurred at the NbZr1 side, indicating good bonding strength at the interface. Fractured samples exhibited intergranular and transgranular fracture morphologies, demonstrating a brittle fracture.

For future research, the effects of thermomechanical post-processing (e.g., heat treatment) on the microstructures and mechanical properties of additively-manufactured NbZr1-Ti6Al4V BS will be investigated.

CRediT authorship contribution statement

Sainand Jadhav: Methodology, Data curation, Writing – original draft, Visualization. Mahdi Sadeqi Bajestani: Methodology, Depositing, Writing – original draft. Saiful Islam: Visualization, Writing – review & editing. Md Abdul Karim: Writing – review & editing. Chang-Jong Kim: Writing – review & editing. Ho-Jin Lee: Writing – review & editing. Young Tae Cho: Writing – review & editing. Duck Bong Kim: Conceptualization, Writing – review & editing, Supervision, Project administration, Funding acquisition.

Declaration of Competing Interest

The authors declare that they have no known competing financial interests or personal relationships that could have appeared to influence the work reported in this paper.

Data availability

Data will be made available on request.

Acknowledgements

The authors of this paper appreciate the continuous support provided by the Center for Manufacturing Research (CMR) and the Department of Manufacturing and Engineering Technology at Tennessee Technological University. This material is based upon work supported by the National Science Foundation under Grant No. 2141905.

References

- A. Bandyopadhyay, Y. Zhang, B. Onuike, Additive manufacturing of bimetallic structures, Virtual Phys. Prototyp. 17 (2022), https://doi.org/10.1080/ 17452759.2022.2040738.
- [2] A. Sarkar, R. Kapoor, A. Verma, J.K. Chakravartty, A.K. Suri, Hot deformation behavior of Nb–1Zr–0.1C alloy in the temperature range 700–1700° C, J. Nucl. Mater. 422 (2012), https://doi.org/10.1016/j.jnucmat.2011.11.064.
- [3] M. Parise, D. Passarelli, J. Bernardini, Niobium to titanium electron beam welding for SRF cavities, arXiv Prepr. arXiv (2022), https://doi.org/10.48550/ arXiv.2209.02503.
- [4] A.M. Beese, B.E. Carroll, Review of mechanical properties of Ti-6Al-4V made by laser-based additive manufacturing using powder feedstock, JOM 68 (2016), https://doi.org/10.1007/s11837-015-1759-z.
- [5] M.J. Torkamany, F.M. Ghaini, R. Poursalehi, Dissimilar pulsed Nd: YAG laser welding of pure niobium to Ti–6Al–4V, Mater. Des. 53 (2014), https://doi.org/ 10.1016/j.matdes.2013.07.094.
- [6] R.H. de Mota Siqueira, I. Atilio, C.C. de Andrade Ferreira, S.M. De Carvalho, M.S. F. De Lima, Fiber laser beam welding between niobium and titanium, J. Aircr. Spacecr. Technol. 4 (2020), https://doi.org/10.3844/jastsp.2020.21.25.
- [7] F. Franchini, P. Pierantozzi, Electron beam welding of dissimilar materials: niobium-base alloy C-103 with titanium-base alloy Ti-6AI-4V ELI, Weld. Int. 6 (1992), https://doi.org/10.1080/09507119209548287.
- [8] X. Gao, J. Liu, L. Zhang, Effect of heat input on microstructure and mechanical properties of pulsed laser welded joints in Ti6Al4V/Nb dissimilar alloys, Int. J. Adv. Manuf. Technol. 94 (2018), https://doi.org/10.1007/s00170-017-1134-z.
- [9] X. Gao, J. Liu, L. Zhang, Dissimilar metal welding of Ti6Al4V and Inconel 718 through pulsed laser welding-induced eutectic reaction technology, Int. J. Adv. Manuf. Technol. 96 (2018), https://doi.org/10.1007/s00170-018-1633-6.
- [10] T. Shehbaz, M. Junaid, F.N. Khan, J. Haider, Dissimilar P-TIG welding between Inconel 718 and commercially pure Titanium using niobium interlayer, Proc. Inst.

- Mech. Eng. Part E J. Process Mech. Eng. 236 (2022), https://doi.org/10.1177/
- [11] C. Zhang, H. Yu, D. Sun, W. Liu, Fabrication of multi-material components by wire arc additive manufacturing, Coatings 12 (2022), https://doi.org/10.3390/ coatings12111683.
- [12] W.E. Frazier, Metal additive manufacturing: a review, J. Mater. Eng. Perform. 23 (2014), https://doi.org/10.1007/s11665-014-0958-z.
- [13] S.W. Williams, F. Martina, A.C. Addison, J. Ding, G. Pardal, P. Colegrove, Wire + arc additive manufacturing, Mater. Sci. Technol. 32 (2016), https://doi.org/10.1179/1743284715Y.0000000073.
- [14] Y. Li, C. Su, J. Zhu, Comprehensive review of wire arc additive manufacturing: hardware system, physical process, monitoring, property characterization, application and future prospects, Results Eng. 13 (2022), https://doi.org/10.1016/ i.rineng.2021.100330.
- [15] M.R. Ahsan, G. Seo, X. Fan, P.K. Liaw, S. Motaman, C. Haase, D.B. Kim, Effects of process parameters on bead shape, microstructure, and mechanical properties in wire arc additive manufacturing of Alo. 1CoCrFeNi high-entropy alloy, J. Manuf. Process. 68 (2021), https://doi.org/10.1016/j.jmapro.2021.06.047.
- [16] ALB Materials, Niobium-Zirconium Alloy Wire- ALB-N017. (https://www.albmaterials.com/metals-and-alloys/727-niobium-zirconium-nb1zr-alloy-wire.html). (Accessed June 2023). (2023).
- [17] S. Islam, M.R. Ahsan, G. Seo, H. Lee, T. Park, F. Pourboghrat, D.B. Kim, Investigations of microstructure and mechanical properties in wire arc additively manufactured niobium-zirconium alloy, Adv. Eng. Mater. (2023), https://doi.org/ 10.1002/adem.202201633.
- [18] P. Bocchetta, L. Chen, J.D.C. Tardelli, A.Cd Reis, F. Almeraya-Calderón, P. Leo, Passive layers and corrosion resistance of biomedical Ti-6Al-4V and β-Ti alloys, Coatings 11 (2021), https://doi.org/10.3390/coatings11050487.
- [19] H. Okamoto, M.E. Schlesinger, E.M. Mueller, ASM Handbook Volume 3: Alloy Phase Diagrams, ASM International, 2016 (ISBN: 978-1-62708-070-5).
- [20] M.J. Torkamany, F.M. Ghaini, R. Poursalehi, An insight to the mechanism of weld penetration in dissimilar pulsed laser welding of niobium and Ti-6Al-4V, Opt. Laser Technol. 79 (2016), https://doi.org/10.1016/j.optlastec.2015.11.005.
- [21] M.J. Torkamany, F.M. Ghaini, R. Poursalehi, A. Kaplan, Combination of laser keyhole and conduction welding: dissimilar laser welding of niobium and Ti-6Al-4V, Opt. Lasers Eng. 79 (2016), https://doi.org/10.1016/j.optlaseng.2015.11.001.
- [22] G.L. Chen, X.T. Wang, K.Q. Ni, S.M. Hao, J.X. Cao, J.J. Ding, X. Zhang, Investigation on the 1000, 1150 and 1400° C isothermal section of the Ti6Al4Nb system, Intermetallics 4 (1996), https://doi.org/10.1016/0966-9795(95)00012-N.
- [23] ASTM B392–18, Standard Specification for Niobium and Niobium Alloy Strip, Sheet, and Plate, West Conshohocken, PA, 2018. DOI: (10.1520/B0393–18).